

Two distinct ancient components in the Sculptor Dwarf Spheroidal Galaxy: First Results from DART¹

Eline Tolstoy², M.J. Irwin³, A. Helmi², G. Battaglia², P. Jablonka⁴, V. Hill⁴, K.A. Venn⁵, M.D. Shetrone⁶, B. Letarte², A.A. Cole², F. Primas⁷, P. Francois⁴, N. Arimoto⁸, K. Sadakane⁸, A. Kaufer⁹, T. Szeifert⁹, T. Abel¹⁰,

ABSTRACT

We have found evidence for the presence of two distinct ancient stellar components (both ≥ 10 Gyr old) in the Sculptor dwarf spheroidal galaxy. We used the ESO Wide Field Imager (WFI) in conjunction with the VLT/FLAMES spectrograph to study the properties of the resolved stellar population of Sculptor out to and beyond the tidal radius. We find that two components are discernible in the spatial distribution of Horizontal Branch stars in our imaging, and in the [Fe/H] and v_{hel} distributions for our large sample of spectroscopic measurements. They can be generally described as a “metal-poor” component ([Fe/H] < -1.7) and a “metal-rich” component ([Fe/H] > -1.7). The metal-poor stars are more spatially extended than the metal-rich stars, and they also appear to be kinematically distinct. These results provide an important insight into the formation processes of small systems in the early universe and the conditions found there. Even this simplest of galaxies appears to have had a surprisingly complex early evolution.

¹Based on FLAMES and UVES observations collected at the European Southern Observatory, proposals 71.B-0641 and 171.B-0588

²Kapteyn Institute, University of Groningen, Postbus 800, 9700AV Groningen, the Netherlands

³Institute of Astronomy, University of Cambridge, Madingley Road, Cambridge CB3 0HA, UK

⁴Observatoire de Paris, section de Meudon, 5 Place Jules Janssen, F-92195 Meudon cedex, France

⁵Macalester College, Saint Paul, MN 55105, USA

⁶University of Texas, McDonald Observatory, USA

⁷European Southern Observatory, Karl-Schwarzschild str 2, D-85748 Garching bei München, Germany

⁸National Astronomical Observatory, 2-21-1 Osawa, Mitaka, Tokyo 181-8588, Japan

⁹European Southern Observatory, Alonso de Cordova 3107, Santiago, Chile

¹⁰Penn State University, State College, PA, USA

Subject headings: dwarf galaxies: general — dwarf galaxies: individual (Sculptor Dwarf Spheroidal)

1. Introduction

The Sculptor (Scl) Dwarf Spheroidal galaxy (dSph) is a close companion of the Milky Way at high galactic latitude ($b = -83^\circ$). Located at a distance of 72 ± 5 kpc (Kunkel & Demers 1977), with $v_{hel} = 109.9 \pm 1.4$ km/s (Queloz, Dubath & Pasquini 1995) it has a low total (dynamical) mass, $1.4 \pm 0.6 \times 10^7 M_\odot$ (Queloz et al. 1995). Irwin & Hatzidimitriou (1995) made the first modern comprehensive determination of the physical properties of Scl. They determined a core radius, $r_c = 5.8 \pm 1.6$ arcmin, and a tidal radius, $r_t = 76 \pm 5$ arcmin with a position angle of 99 ± 1 degrees, and confirmed it to be a moderately luminous galaxy in the dSph class ($M_V = -10.7 \pm 0.5$), with a modest central surface brightness ($\Sigma_{o,V} = 23.5 \pm 0.5$ mag/arcsec²). Like most dSph galaxies Scl does not appear to have much, if any, HI gas (e.g., Bouchard, Carignan & Mashchenko 2003).

Observations of Scl have revealed a sizeable population of RR Lyrae variable stars (e.g., Kaluzny et al. 1995), clearly indicating that its stellar population contains a globular cluster age component. Scl also shows tantalizing evidence in its extended horizontal branch (HB) for an unusual enrichment history (e.g., Hurley-Keller, Mateo & Grebel 1999; Majewski et al. 1999). Monkiewicz et al. (1999) have detected stars several magnitudes below the oldest possible main-sequence turn-offs. Their accurate photometry allowed them to conclude that the mean age of Scl is similar to that of a globular cluster, but that there is an age spread within this epoch indicative of an extended star formation history. Thus the entire star formation history of Scl apparently lasted only a few Gyr, and after this initial period of activity more than 10 Gyr ago Scl appears to have been dormant.

There have been several previous spectroscopic studies of individual stars in Scl, firstly to determine the kinematic properties (e.g., Armandroff & Da Costa 1986; Aaronson & Olszewski 1987; Queloz et al. 1995) which have indicated a moderate mass-to-light ratio $M/L = 9 \pm 6 (M/L_V)_\odot$. This value is significantly higher than that typical for a globular cluster, but much lower than found for many dSphs (e.g., Draco and Ursa Minor). There have also been studies of the abundances of small samples of individual Red Giant Branch (RGB) stars at low and high resolution (Shetrone et al. 2003; Tolstoy et al. 2001, 2003). These stars were selected from the central region of Scl, and although they showed a wider range in [Fe/H] than would be naively expected based on colour-magnitude diagram (CMD) analysis,

no conclusions could be drawn on the large scale spatial variations of these properties.

Here we present the first results from the DART (Dwarf Abundances and Radial velocities Team) large programme at ESO. We present the results for v_{hel} and $[Fe/H]$ measurements from our FLAMES spectroscopy of 401 RGB stars for the first galaxy in our sample, Scl dSph. The relatively high signal/noise, S/N (≈ 10 -20 per pixel) of our data has enabled us to derive both accurate metallicities (≈ 0.1 dex from internal errors) and radial velocities (to $\approx \pm 2$ km/s). This is the first time that a large sample of both types of measurement has been made in a single galaxy. A more detailed description of our data and data reduction techniques will be provided in subsequent papers (Irwin et al. in prep; Hill et al. in prep; Battaglia et al. in prep). Here we provide an overview of our first intriguing results.

2. Observations

2.1. Imaging

The ESO Wide Field Imager (WFI) observations were obtained from the ESO archive for the central region of Scl, and more extended observations of outer fields were made by us. We used the pipeline reduction software developed by the Cambridge Astronomical Survey Unit for processing mosaic camera imaging (Irwin & Lewis 2001; Irwin et al. 2004). These observations were used to study the photometric properties of Scl stars out to the tidal radius and as target selection for VLT/FLAMES observations of stars along the RGB.

2.2. Spectroscopy

All VLT/FLAMES observations were made in Medusa mode, giving ~ 120 fibres to be placed over a 25 arcmin diameter field of view. Most of the observations were taken with the Low Resolution grating LR8 (which includes the Ca II triplet (CaT) lines), apart from the central pointing where High Resolution gratings were used (see Hill et al. in prep). The CaT method is well calibrated to provide an accurate estimate of the $[Fe/H]$ abundance of an RGB star (Rutledge, Hesser & Stetson 1997; Cole et al. 2004) and also to provide an accurate radial velocity measurement. The FLAMES fields were placed at varying distances from the centre of the galaxy to beyond the tidal radius.

The FLAMES data were all reduced, extracted and wavelength calibrated using the

GIRBLDRS pipeline¹ provided by the FLAMES consortium (Geneva Observatory, Blecha et al. 2003). For sky subtraction, velocity and equivalent width (EW) estimation, we developed our own software which was thoroughly checked on multiple observations of the same fields taken at different times. Wavelength shifts were generally found to be negligible ($\approx \pm 1$ km/s). Each target spectrum was automatically continuum-corrected and cross-correlated with a zero-continuum Gaussian model CaT template. With a velocity determined it is then straightforward to estimate the EW of the individual CaT lines. We found that for reliable [Fe/H] determinations from CaT calibrations a $S/N \geq 10$ is required, and for reliable v_{hel} a $S/N \geq 7.5$ is sufficient. All the plots in this paper use the $S/N > 10$ data set, as we always consider both the [Fe/H] and the v_{hel} measurements.

We were able to verify the zero point accuracy for both velocity and abundance determinations by comparison with independent previous measurements of stars in Scl, which we had deliberately reobserved. We also have overlap between our own HR and LR samples to verify consistency of velocity and [Fe/H] measurements using different gratings and based on different abundance determination methods.

3. Analysis

3.1. Spatial Distribution

Previous studies have already suggested that the spatial distribution of the Horizontal Branch stars in Scl shows signs of a population gradient, with the red horizontal branch stars (RHB) being more tightly concentrated than the blue horizontal branch (BHB) stars (e.g., Hurley-Keller et al. 1999; Majewski et al. 1999). Unlike previous wide field studies, our WFI imaging data extends beyond the nominal tidal radius and with an average $5\text{-}\sigma$ limiting magnitude of $V=23.5$ and $I=22.5$ also probes well below the horizontal branch. This has enabled us to unequivocally demonstrate that the BHB and RHB stars have markedly different spatial distributions (see Figure 1).

These RHB and BHB populations were selected from the WFI CMD shown in Figure 2 using the selection boxes marked. It is clear that the BHB region is almost completely uncontaminated by foreground stars, whereas the RHB zone includes a significant underlying foreground component. To make a quantitative estimate of the contamination of the RHB sample by foreground stars we selected a region of similar CMD foreground occupancy, well away from the Scl stellar locus (also outlined in Figure 2). The radial density distributions

¹available at SourceForge, <http://girbldrs.sourceforge.net/>

of the RHB component were then corrected by the expected foreground contamination and the results for both the RHB and BHB distributions together with their density ratio as a function of radial distance, are shown in the lower panels of Figure 1. The different spatial occupancy of the two populations is striking and provides strong evidence that we are seeing two distinct components. The characteristics of the BHB and RHB are also consistent with different ages (e.g., ≤ 2 Gyr), or different metallicities ($\Delta[\text{Fe}/\text{H}] \sim 0.7$ dex), from theoretical modelling of globular cluster horizontal branches by Lee et al. (2001).

3.2. Metallicity Distribution

Our VLT/FLAMES spectroscopic sample provides measurements of $[\text{Fe}/\text{H}]$ for 401 individual candidate RGB-selected stars with final $\text{S}/\text{N} > 10$, of which 308 have a high membership probability (these are plotted in Figure 3), defined to be $80 \text{ km/s} < v_{hel} < 150 \text{ km/s}$ i.e., approximately within 3σ of v_{sys} (see Figure 4). At the high Galactic latitude of Scl v_{hel} is a good estimator of membership probability assuming $v_{sys} = 110 \text{ km/s}$, and $\sigma \approx 10 \text{ km/s}$.

For those RGB stars which were determined to have a high probability of membership, we show the distribution of $[\text{Fe}/\text{H}]$ measurements as a function of elliptical radius (the equivalent distance along the semi-major axis) from the centre of Scl in the upper panel of Figure 3. A well-defined metallicity gradient is apparent with a similar scale size to the RHB versus BHB spatial distributions. The lower panel of this figure highlights the abrupt change in the $[\text{Fe}/\text{H}]$ distribution that occurs at about $r = 0.2 \text{ deg}$ ($2r_c$) and also the broad range in $[\text{Fe}/\text{H}]$ over the whole galaxy. Although both inner and outer distributions cover a broad range of values, the inner is centred at $[\text{Fe}/\text{H}] = -1.4$ with a range of $\pm 0.6 \text{ dex}$ and the outer distribution is centred at $[\text{Fe}/\text{H}] = -2$ with a similar range of $\pm 0.6 \text{ dex}$. The drop in $\langle [\text{Fe}/\text{H}] \rangle$ at $2r_c$ from the centre also corresponds to the transition between the dominance of the RHB and BHB populations seen in Figure 1. This is not seen if the colour of the RGB alone is taken as an indication of metallicity.

3.3. Kinematics

In the upper panel of Figure 4 we plot the sample of v_{hel} measurements versus elliptical radius for which the continuum $\text{S}/\text{N} > 10$. The distinction between foreground stars and members of Scl is generally unambiguous. The clustering around the systemic velocity of $v_{sys} = 110 \text{ km/s}$ is clear and is highlighted by the dashed line and the dotted 3σ deviation limits. Although present, foreground contamination can be seen to be almost negligible,

even in the outer regions, which simplifies subsequent analysis.

We have divided our “member” sample into metal-poor ($[\text{Fe}/\text{H}] < -1.7$) and metal-rich ($[\text{Fe}/\text{H}] > -1.7$) distributions. This difference is quantified in the lower panels of Figure 4 which shows the v_{hel} distributions over three radial zones for the different metallicity components separately. The variation in v_{sys} and σ in these three regions is computed using the maximum likelihood approach described in Hargreaves et al. (1994), but modified to directly compute the likelihood function over a 2D search grid. We found that v_{sys} does not vary significantly between different populations or regions, but σ does (see Figure 4).

One obvious feature of the velocity distributions is the difference in the kinematic properties of the two metallicity components. In general the more metal poor component has a higher velocity dispersion than the more metal rich component. This difference is most striking in the central panel ($0.2^\circ < r < 0.5^\circ$) of the triptych where σ is 11.0 ± 1.0 km/s and 6.8 ± 0.8 km/s respectively. The swap in the dominance of the components is stark in the outer zone ($r > 0.5$), where there are hardly any stars at all in the metal-rich category and provides compelling evidence that we are indeed observing two dynamically different components in Scl.

4. Conclusions

Our FLAMES results show that Scl contains two distinct stellar components, one metal-rich, $-0.9 > [\text{Fe}/\text{H}] > -1.7$, and one metal-poor, $-1.7 > [\text{Fe}/\text{H}] > -2.8$. The metal-rich population is more centrally concentrated than the metal poor, and on average appears to have a lower velocity dispersion, $\sigma_{metal-rich} = 7 \pm 1$ km/s, whereas $\sigma_{metal-poor} = 11 \pm 1$ km/s (see Figure 4). Our WFI results show that there is a comparable difference over the same scale in the spatial distribution of BHB stars and RHB stars. Plausibly combining these results enables us to distinguish these two distinct components on the basis of kinematics (Figure 4), metallicity (Figure 3) and spatial distribution (Figure 1). These large samples allow us for the first time to quantify these large scale trends in a statistically meaningful fashion.

There are indications that this is a common feature of dSph galaxies. Our preliminary analysis of v_{hel} and $[\text{Fe}/\text{H}]$ measurements in the other galaxies in our sample (Fornax and Sextans dSph, Battaglia et al., in prep) also shows very similar characteristics to Scl, especially in the most metal poor component. The mix of populations between the inner and outer regions is clearly changing. The radial velocity studies of Wilkinson et al. (2004) and Kleyna et al. (2004) have also considered the possibility that kinematically distinct

components exist in Ursa Minor, Draco and Sextans.

What mechanism could create two ancient stellar components in a small dwarf spheroidal galaxy? A simple possibility is that the formation of these dSph galaxies began with an initial burst of star formation, resulting in a stellar population with a mean $[\text{Fe}/\text{H}] \leq -2$. Subsequent supernovae explosions from this initial episode could have been sufficient to cause gas (and metal) loss such that star formation was inhibited until the remaining gas could sink deeper into the centre and begin star formation again (e.g., Mori, Ferrara & Madau 2002). Thus the subsequent generation(s) of stars would inhabit a region closer to the centre of the galaxy, and have a higher average metallicity (≥ -1.4) and different kinematics. Another possible cause is external influences, such as minor mergers, or accretion of additional gas. It might also be that events surrounding the Epoch of Reionisation, strongly influenced the evolution of these small galaxies (e.g., Bullock, Kravtsov & Weinberg 2001) and resulted in the stripping or photoevaporation of the outer layers of gas in the dSph, meaning that subsequent more metal enhanced star formation occurred only in the central regions.

The full abundance analysis of the FLAMES HR data (Hill et al. in prep) will provide more details of the chemical enrichment history of Scl. This will hopefully enable us to distinguish between two episodes of star formation, each of which created the separate kinematic components seen here, or more continuous star formation, manifested as a gradient in velocity dispersion and metallicity from the centre of the galaxy.

Here we have shown that even dSphs, the smallest galactic systems, did not form simply, as might be assumed. The wealth of data presented here points to the presence of dynamically distinct components in these galactic building blocks, or templates, and provides a stimulus to theories of the formation and evolution of dSphs.

ET gratefully acknowledges support from a fellowship of the Royal Netherlands Academy of Arts and Sciences, and thanks Renzo Sancisi for a careful reading of the draft. KAV thanks the NSF for support through a CAREER award, AST-9984073. MDS would like to thank the NSF for partial support under AST-0306884.

REFERENCES

- Aaronson M. & Olszewski E.W. 1987 AJ, 94, 657
Armandroff T.E. & Da Costa G.S. 1986 AJ, 92, 777

- Blecha A., North P., Royer F. & Simond, G. 2003 *BLDR Software Reference Manual 1.09*, Doc. No. VLT-SPE-OGL-13730-0040
- Bouchard A., Carignan C. & Mashchenko S. 2003 *AJ*, 126, 1295
- Bullock J.S., Kravtsov A.V. & Weinberg D.H. 2001 *ApJ*, 548, 33
- Cole A.A., Smecker-Hane T.A., Tolstoy E., Bosler T.L. & Gallagher J.S. 2004 *MNRAS*, 347, 367
- Hargreaves J.C., Gilmore G., Irwin M.J. & Carter D. 1994 *MNRAS*, 269, 957
- Hurley-Keller D., Mateo M., & Grebel E.K. 1999 *ApJL*, 523, 25
- Irwin M. & Lewis J. 2001 *NewAR*, 45, 105
- Irwin M. et al. 2004, *Proc. SPIE* **5493**
- Irwin M. & Hatzidimitriou D. 1995 *MNRAS*, 277, 1354
- Kaluzny J., Kubiak M., Szymanski M., Udalski A., Krzeminski W. & Mateo M. 1995 *A&AS*, 112, 407
- Kleyna et al. 2004 *MNRAS*, in press (astro-ph/0409066)
- Kunkel W.E. & Demers S. 1977 *ApJ*, 214, 21
- Lee Y-W., Yoon S-J., Rey S-C. & Chaboyer B. 2001 *Astrophysical Ages & Time Scales*, eds. T. von Hippel et al.
- Majewski, S.R., Siegel, M.H., Patterson, R.J. & Rood, R. 1999 *ApJL*, 520, 33
- Monkiewicz J., Mould J.R., Gallagher J.S., Clarke J.T., Trauger J.T., Grillmair C. & WFPC2 IDT 1999 *PASP*, 111, 1392
- Queloz D., Dubath P. & Pasquini L. 1995 *A&A*, 300, 31
- Rutledge G.A., Hesser J.E. & Stetson P.B. 1997 *PASP*, 109, 907
- Shetrone M.D., Venn K., Tolstoy E., Primas F., Hill V. & Kaufer A. 2003 *AJ*, 125, 684
- Tolstoy E., Irwin M.J., Cole A.A., Pasquini L., Gilmozzi R. & Gallagher J.S. 2001 *MNRAS*, 327, 918
- Tolstoy E., Venn K., Shetrone M.D., Primas F., Hill V., Kaufer A. & Szeifert T. 2003 *AJ*, 125, 684

Wilkinson M., Kleyana J.T., Evans N.W., Gilmore G., Irwin M.J. & Grebel E.K. 2004 ApJL, 611, 21

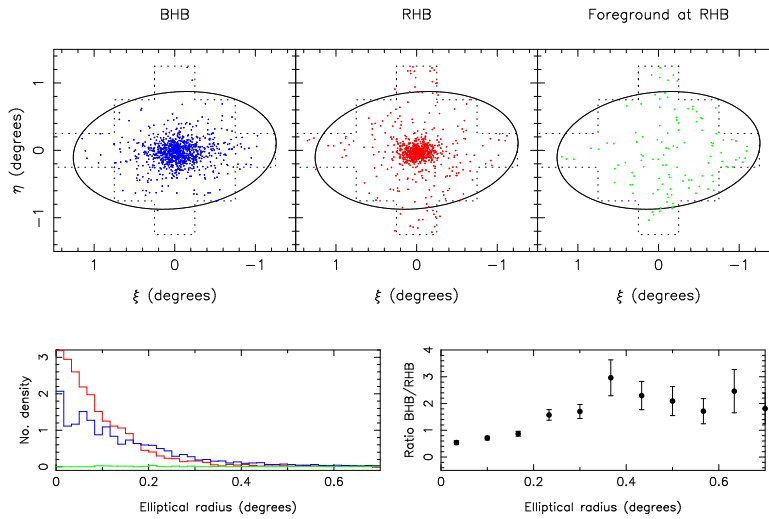


Fig. 1.— The distribution of Horizontal Branch stars from WFI imaging of the Scl dSph. The upper panels show the different spatial distributions of blue horizontal branch stars (BHB), and red horizontal branch stars (RHB) as selected from the M_v , $V-I$ Colour-Magnitude Diagram (CMD) shown in Figure 2. Also shown, to illustrate the foreground contamination in the RHB distribution, are a CMD-selected sample of foreground stars to match the RHB contamination density (see Figure 2). The ellipse is the tidal radius of Scl as defined by Irwin & Hatzidimitriou (1995). The lower panels quantitatively show the spatial variation of number density per unit area of these three population components (BHB in blue, RHB in red and foreground in green) and the ratio of BHB to RHB number densities after correcting the RHB component for foreground contamination. The physical scale at the distance of Sculptor is 1 degree to 1.4 kpc.

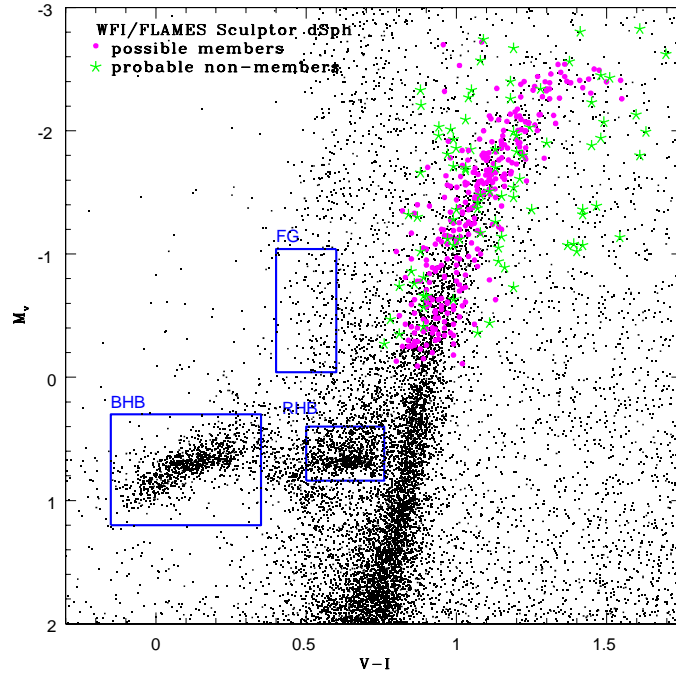


Fig. 2.— The Colour-Magnitude Diagram for the WFI coverage of Scl shown in Figure 1. The green and magenta symbols are the Red Giant Branch stars which were observed with VLT/FLAMES and for which we have accurate v_{hel} and $[Fe/H]$ measurements ($S/N > 10$). The potential members of Scl are shown as magenta dots and non-members shown as green stars. Also shown are the regions used to define the BHB, RHB and foreground comparison sample (FG).

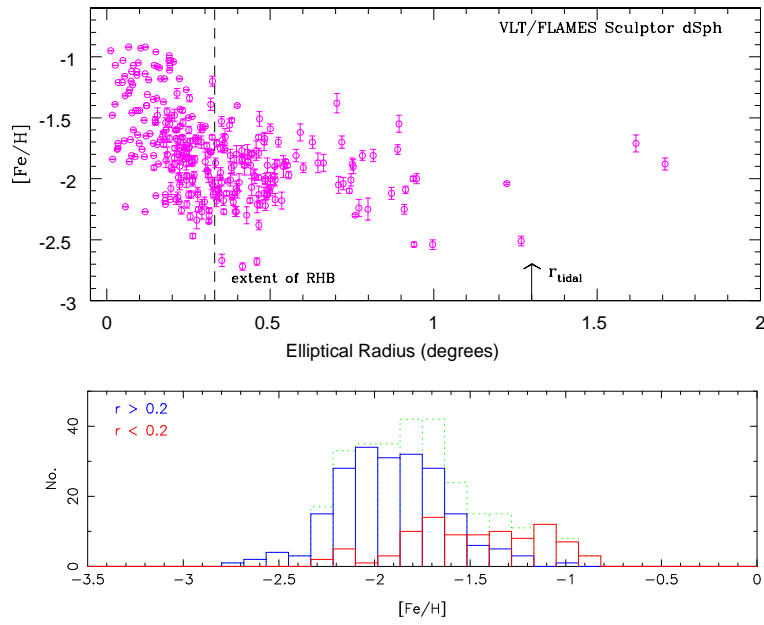


Fig. 3.— VLT/FLAMES spectroscopic measurements of $[\text{Fe}/\text{H}]$ for the 308 potential RGB velocity members of Scl versus radius (top panel). The lower panel shows the distribution of $[\text{Fe}/\text{H}]$ for: the entire sample of Scl member RGB stars (dotted line); the 97 stars within the central, $r=0.2$ degree region (red solid line); and the 211 stars beyond $r>0.2$ degrees (blue solid line).

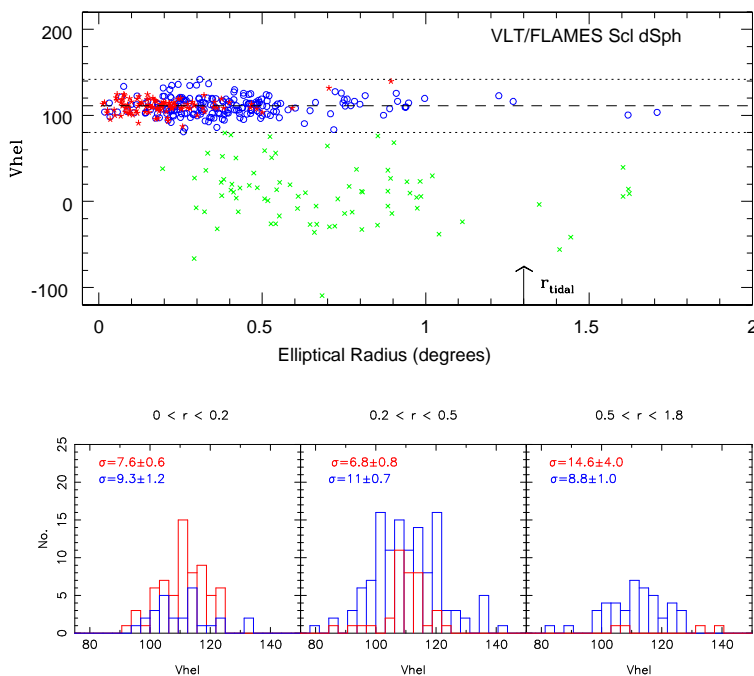


Fig. 4.— The top panel shows v_{hel} as a function of elliptical radius for all stars satisfying $S/N > 10$. The 308 stars which are potential members are plotted as red stars ($[Fe/H] > -1.7$) and blue circles ($[Fe/H] < -1.7$), while the 93 green crosses are assumed to be non-members. The lower panels quantify how the velocity distribution changes as a function of metallicity and radius. The low metallicity distribution is plotted in blue, and the higher metallicity in red, as in the upper panel.